Extracting Continuum Electron Dynamics from High Harmonic Emission from Molecules

R. M. Lock, S. Ramakrishna, X. Zhou, H. C. Kapteyn, M. M. Murnane, and T. Seideman

Phys. Rev. Lett. **108**, 133901 — Published 26 March 2012

DOI: 10.1103/PhysRevLett.108.133901

Extracting continuum electron dynamics from high harmonic emission from molecules

R.M. Lock,[1] S. Ramakrishna,[2] X. Zhou[1], H.C. Kapteyn[1,] M.M. Murnane[1], and T. Seideman[2]

[1]*Department of Physics and JILA, University of Colorado and NIST, Boulder, CO 80309, USA*

[2]*Department of Chemistry, Northwestern University, Evanston, IL 60208, USA*

Corresponding author: Robynne.Lock@jila.colorado.edu

We show that high harmonic generation is the most sensitive probe of rotational wavepacket revivals, revealing very high order rotational revivals for the first time using any probe. By fitting high-quality experimental data to an exact theory of high harmonic generation from aligned molecules, we can extract the underlying electronic dipole elements for high harmonic emission and uncover that the electron gains angular momentum from the photon field.

In recent years, there has been increasing interest in studying high-order harmonic generation (HHG) from coherently aligned molecules as a potential approach for extracting dynamic molecular structure [1-18]. In these experiments, a pump pulse creates a rotational coherence in a molecular gas, inducing nonadiabatic alignment through the interaction of a short, intense, laser pulse with the anisotropic polarizability of the molecule. The induced rotational wavepacket manifests itself in periodic quantum revivals and fractional revivals of the alignment distribution that create transient alignment and anti-alignment of the molecular sample at certain times after the pump pulse. Revivals occur at fractions of the rotational period of the molecule [19-21], with their positions and nature determined by symmetry of the molecule and by the excited angular momentum states. A more intense time-delayed pulse then generates harmonics from the sample [2-4].

Past work exploring HHG from impulsively aligned molecules concentrated primarily on extracting structural information by characterizing variations in HHG intensity as the rotational distribution experiences low-order rotational revivals (full, ½, and ¼; ¾). HHG emission can be understood to a first approximation in a semi-classical three-step model in which a strong laser field ionizes an electron from the molecule. The electron then propagates in the laser field, and if it oscillates back to the vicinity of the parent cation, it can recombine with the molecule and emit coherent HHG beams [22]. Both the ionization and recombination steps in HHG are sensitive to the molecular orbital structure and orientation. Past work demonstrated that the intensity, phase and polarization of the HHG emission are sensitive to the orbital structure of the molecule [10], as well as to the coherence properties and the revival pattern of the rotational wavepacket [23, 24].

In this work, through high-fidelity measurements of HHG emission from molecules, we observe and analyze higher order fractional rotational revivals (up to the 1/16) for the first time. These observations demonstrate that HHG is the most sensitive probe of rotational wavepacket dynamics, allowing us to uncover new insights not observable using conventional probes. Using a two-center model of the molecule, we can intuitively explain how the observed high harmonic emission is related to the alignment distribution, and extract the pump laser intensity and the rotational temperature of the medium. More remarkably, by comparing a rigorous theory of HHG from aligned molecules [23, 24] with high signal-to-noise experimental data, we can extract the underlying electronic dipole elements of the HHG signal, as well as information on

the continuum electron dynamics. Specifically, we uncover that the continuum electron gains angular momentum from the photon field while propagating in the continuum, and that only a small number of electron partial waves strongly dominate the HHG dynamics. For molecules with antisymmetric ground state orbitals, electrons liberated with low electronic angular momentum l=1 recombine from a higher angular momentum state with l=3. Such electronic angular momentum non-conserving events dominate over angular momentum conserving events, increasingly so as the harmonic order increases, for both CO_2 and N_2O. Thus, attosecond electron dynamics manifests itself in the experimental observable of higher-order fractional rotational revivals and is crucial for their observation.

In our experiments, we used a Ti:sapphire laser-amplifier system producing ~25 fs pulses at 800 nm wavelength, running at a 1 kHz repetition rate. The laser output is split into pump and probe beams. The pump pulse is stretched to ~120 fs using material dispersion and then focused into a continuous supersonic gas jet of CO_2 or N_2O to excite a rotational wavepacket. The probe beam is then focused into the gas jet to generate harmonics. The focus of the probe beam is placed slightly before the gas jet so that the divergence of the beam selects for optimum phase matching of only the short electron trajectories [25]. The intensities of the pump and probe beams are ~2-6 x 10^{13} W/cm^2 and ~1-2 x 10^{14} W/cm^2, respectively. The beams are linearly polarized parallel to each other. The gas jet is a ~150 μm diameter tube, continuously backed with gas at a pressure of ~700 torr. The estimated rotational temperature of the molecules is ~60-100 K. The HHG spectrum is captured using an EUV spectrometer and an EUV CCD camera.

Figure 1(a, b) plots the intensity of the 31st harmonic generated in CO_2 as a function of time delay between pump and probe pulses (solid black line) along with fits using the two-center interference model [9, 15, 26, 27] (dashed red line) and the exact theory of [23, 24] (dotted blue line). Small revivals, previously unreported in CO_2, are clearly visible at time delays corresponding to $^1/_{16}$, $^1/_{12}$ and $^1/_6$ of the rotational period, along with the $^1/_8$ revival, and at integer multiples of those time delays. Figure 2 plots similar measurements and fits for the 25th harmonic from N_2O molecules. The ½ revival of N_2O has been studied previously [15, 17], but new features are clearly visible at $^1/_6$, ¼, $^1/_3$, $^2/_3$, ¾, and $^5/_6$ of the rotational period.

The time-dependent molecular alignment distribution following impulsive excitation can be calculated with a high degree of confidence, with the major uncertainty being the intensity of

the exciting laser pulse and the rotational temperature of the molecular sample [19-21]. Simple, phenomenological approximations can be used to describe the rotational angular distribution, by assuming $\langle \cos^2 \theta \rangle$ or $\langle \sin^2 2\theta \rangle$ alignment parameters, where θ is the angle between the aligning field and the molecular axis [2, 4], and $\langle \cos^2 \theta \rangle = 1$ corresponds to perfect alignment. Recent calculations described rotational revivals in terms of cosine moments $\langle \cos^N \theta \rangle$ [28]. Higher order cosine-moments up to $N=8$ can well describe the locations of the new revivals observed in our data.

To intuitively understand our data, the rotational angular distribution can be integrated with the two-center interference model, where the dependence of the HHG emission on the molecular structure and alignment arises predominantly from interferences in the recombination step [26, 27]. While by no means complete, this model can provide useful physical insight. The two-center interference model was initially introduced to describe a spectral minimum that appears as a function of harmonic order. However, this model also predicts a minimum in HHG emission as a function of alignment angle and therefore can describe HHG as the molecular alignment changes with pump-probe time delay. In previous work we showed that the two-center interference model can well describe HHG from CO_2 and N_2O during the ¾ and ½ revivals [9, 15]. HHG from the full and ½ revivals of CO_2 and N_2O is anti-correlated with $\langle \cos^2 \theta \rangle$: for the internuclear distances and molecular orbital shapes in these two molecules, destructive interference between recombination to the two centers of electron density occurs when the molecular axis is aligned along the laser polarization direction. The highest occupied molecular orbitals of CO_2 and N_2O are both antisymmetric, and thus the HHG amplitude from a perfectly aligned molecule in the two-center model is given by -

$$H(\theta) = A \sin(\frac{\pi R}{\lambda} \cos\theta), \qquad (1)$$

where A is a scaling factor, R is the distance between centers of electron density, λ is the wavelength of the recombining electron, and θ is the angle between the ionizing field polarization vector and the molecular axis. To obtain the harmonic intensity from molecules distributed over a range of angles, the HHG from a perfectly aligned molecule must be integrated with the angular distribution, which serves as a weight factor over the alignment angle θ. The harmonic yield for a given angular distribution is then -

$$I(t) = \left| \int_0^{\pi/2} H(\theta)\rho(\theta,t)\sin\theta d\theta \right|^2 + C, \qquad (2)$$

where $\rho(\theta,t)$ is the rotational angular distribution, t is the time delay between the alignment and ionization pulses and C is included for background compensation. Fits to this model for CO_2 and N_2O are shown as the dashed red lines in Figures 1 and 2 respectively. The fits were obtained through a least-squares fitting procedure with A, $B(=R/\lambda)$, and C as the fit parameters. Using the values of B extracted from the fitting procedure and the value of λ for each harmonic order, we extracted the value of R for each molecule. For CO_2, R = 0.241 ± 0.010 nm, while for N_2O R = 0.229 ± 0.021 nm. These values are in agreement with the known distances between centers of electron density 0.232 nm and 0.231 nm for CO_2 and N_2O, respectively. The wavelength of the recombining electron λ used in the calculation was obtained using the dispersion relationship $E_k=nhv$, where E_k is the energy of the recombining electron and nhv is the harmonic energy. Thus, the two-center model can be fit to the general features of all revivals present and also indicates the presence of even higher order fractional revivals hinted-at in the data at amplitude near the experimental noise level. As shown in the supporting information, it can also extract the rotational temperature and pump laser intensity.

Considerable further insight is gained by accounting for angular momentum exactly using the theory of [23, 24], which allows us to extract the electron dipole moments, and also uncover new insight into the electron dynamics of molecular HHG. We start with the expression for the expectation value of the time-dependent induced dipole in a direction parallel to the polarization of the probe pulse [23],

$$\langle \psi(t)|\vec{\mu}\cdot\hat{n}|\psi(t)\rangle = \int d\hat{R}\rho(\hat{R};\tau)\Big\{\cos^2\theta \sum_{l,l',k_l} Y_{lk_l}(\hat{R})Y^*_{l'k_l}(\hat{R})F_{\|}(l,l',k_l,t)$$

$$+\sin^2\theta \sum_{l,l',k_l} Y_{lk_l}(\hat{R})Y^*_{l'k_l}(\hat{R})F_{\perp}(l,l',k_l,t)\Big\} + c.c \qquad (3)$$

In Eq. (3), $\rho(\hat{R}:\tau)$ is the rotational density matrix, where $\hat{R}=(\theta,\varphi)$ are the Euler angles of rotation of the molecular frame with respect to the laboratory frame and τ is the time delay between the pump and probe pulses. The $Y_{l,kl}$ are spherical harmonics, where the indices l and k_l denote the quantum numbers of the continuum electron angular momentum and its projection on

the molecular axis respectively. The exact expressions for the electronic dipole matrix elements parallel ($F_{\|}$) and ($F_{\perp}$) perpendicular to the molecular axis are provided in Refs. [23, 24]. Physically, each electronic dipole matrix element $F_{\|(\perp)}(l,l',k_l,\Omega)$ can be understood in terms of the familiar three-step process of HHG. It signifies an electron ionized either parallel (||) or perpendicular (□) to the molecular axis into a continuum state that has an angular momentum value of l' about the space fixed z-axis, its propagation and eventual recombination into the ground state from a continuum state of angular momentum l, while the projection of the angular momentum of the continuum electron about the molecular axis given by k_l is conserved. While the theory of [23,24] is exact and explicitly shows the existence and origin of high order fractional rotational revivals, the numerical calculation of the electronic dipole matrix elements is very difficult and hence all existing calculations of HHG from aligned molecules involve significant approximations. At the same time, the combination of a theory that accounts properly for the HHG angular momentum algebra with accurate experiments can yield these elements empirically.

For the purpose of fitting to data, the amplitude of harmonics emitted by molecules with a π_g symmetry, such as CO_2 and N_2O, Eq. (1) is expressed as -

$$\int dt \exp(i\Omega t)\langle\psi(t)|\vec{\mu}\cdot\hat{n}|\psi(t)\rangle = \sum_n (A_{2n}+iB_{2n})\langle\cos^{2n}\theta\sin^2\theta\rangle + \sum_n (C_{2n}+iD_{2n})\langle\cos^{2n}\theta\sin^6\theta\rangle \quad (4)$$

where Ω is the harmonic frequency, *A, B, C* and *D* are the fit parameters to be extracted, and the measured signal is given as the squared absolute value of Equation (4). The coefficients are related to the electronic dipole matrix elements as -

$$A_{2n}+iB_{2n} = \sum_{l+l'\geq 2n}\sum_{k_l=\pm 1} f_{ll'}^{2n}F_{\|}(l,l',k_l,\Omega) + g_{ll'}^{2n}F_{\perp}(l,l',0,\Omega) \quad (5)$$

$$C_{2n}+iD_{2n} = \sum_{l+l'\geq 2n+4}\sum_{k_l=\pm 2} h_{ll'}^{2n}F_{\perp}(l,l',k_l,\Omega) \quad (6)$$

where *f, g* and *h* are known constants, containing the transformation of the spherical harmonics into geometric functions. Angular momentum selection rules allow only for odd values of *l* and *l'* and for π_g symmetry, k_l can take values ± 1 in Eq. (5) and ± 2 in Eq. (6).

In principle, for a given value of n, one can have an infinite number of partial wave (l) contributions. In practice, however, the series of partial waves converges rapidly and higher order angular momentum values become progressively smaller. This result, found numerically in Ref. [23, 24], is substantiated by our experiments below. The constraints $l + l' \geq 2n$ and $l + l' \geq 2n + 4$ consequently lead to truncation also of the series expansion in n. In practice, a fit to reliable data will determine which partial wave continuum functions participate in the electronic dynamics. From Figures 1 and 2 we learn that, in our present experiments, values of n up to n=3 participate in the dynamics while C and D in Eq. (4) are negligible. As a rough initial estimate of the number of partial waves making sufficiently large contributions to be observable, we use calculations within the molecular strong field approximation (SFA). Our results are clearly independent of the validity of the SFA, depending only on the accuracy of the experimental data, but the electronic matrix elements extracted can serve to test the results of the SFA. This procedure yields -

$$A_6 + iB_6 \approx 2 f_{33}^6 F_{\|}(3,3,\pm 1,\Omega) \quad (7)$$

$$A_4 + iB_4 \approx 2 f_{31}^4 F_{\|}(3,1,\pm 1,\Omega) + 2 f_{33}^4 F_{\|}(3,3,\pm 1,\Omega) + g_{31}^4 F_{\perp}(3,1,0,\Omega) \quad (8)$$

$$A_2 + iB_2 \approx 2 f_{11}^2 F_{\|}(1,1,\pm 1,\Omega) + 2 f_{31}^2 F_{\|}(3,1,\pm 1,\Omega) + 2 f_{33}^2 F_{\|}(3,3,\pm 1,\Omega)$$
$$+ g_{11}^2 F_{\perp}(1,1,0,\Omega) + g_{31}^2 F_{\perp}(3,1,0,\Omega) \quad (9)$$

Using the fact that $F_{\|}(1,1,\pm 1,\Omega) = F_{\perp}(1,1,0,\Omega)$ and $F_{\|}(3,1,\pm 1,\Omega) = \frac{1}{p} F_{\perp}(3,1,0,\Omega)$, where p is a constant, one can solve the system of equations (7-9) and obtain estimates for the dominant electronic dipole matrix elements. (The second relationship arises from the fact that the angular parts of the dipole matrix elements depend on the symmetry of the ground state only, while its radial part is influenced by the molecular potential and the ionizing field.)

This theory fully explains the fractional revivals in CO_2 shown in Figure 1 and reveals their physical content: angular momentum theory indicates that $\langle \cos^2\theta \rangle$ exhibits only the ¼ and ½ revivals, since it allows only second-order rotational coherences, whereas $\langle \cos^2\theta \sin^2\theta \rangle$ allows fourth-order rotational coherences and thus also exhibits the 1/8 and 3/8 revivals. Higher

moments, such as $\left\langle \cos^4\theta \sin^2\theta \right\rangle$, can be shown to involve rotational coherences of order six, hence they express themselves as additional revivals such as the 1/12 and 1/6, while the 1/16 and 3/16 revivals emerge from $\left\langle \cos^6\theta \sin^2\theta \right\rangle$, which involves rotational coherences of order eight. As the highest order fractional revival features seen in the present experimental signal are that of the 1/16 and 3/16, it is clear that the electronic dynamics is determined by partial waves up to $l + l' = 6$.

Similarly, for the revivals in N_2O shown in Figure 2, the rotational expectation value $\left\langle \cos^4\theta \sin^2\theta \right\rangle$ is the lowest order in the series that yields fractional revivals at 1/6 and 1/3, whereas the element $\left\langle \cos^6\theta \sin^2\theta \right\rangle$ is responsible for the observed rotational revivals at 1/8 and 3/8 of the rotational period. Hence a similar expansion of Eq. (2) up to *n=3* has been used to obtain the fits shown in Figure 2. *Most interestingly, our ability to apply analytical angular momentum algebraic considerations to correlate each fractional revival with a specific rotational expectation value, and hence a specific electronic dipole element, provides a route to extract the continuum electronic dynamics that underlie the signal from the experimental data.*

Figures 3(a) and (b) show the magnitudes of the electronic dipole elements extracted from our experimental data for N_2O and CO_2 as functions of the harmonic order. Several interesting features of the electronic matrix elements responsible for HHG are apparent. First, while the expansion in Eq. (5) is in principle infinite, only a small number of partial waves *l,l'=1,3* dominate. Second, for both molecules considered here the dominant element is $|F_{\|}(3,1,k_l,\Omega)|$ - signifying ionization into a continuum electronic wave function with angular momentum *l'=1* followed by propagation in the field, during the course of which angular momentum is gained from the photon field, and recombination of partial wave *l=3*. Third, the dominance of the $|F_{\|}(3,1,k_l,\Omega)|$ element over the $|F_{\|}(1,1,k_l,\Omega)|$ and $|F_{\|}(3,3,k_l,\Omega)|$ angular momentum conserving events increases with the harmonic order. We note that the experimental dipole elements follow the same order of dominance that was theoretically found for O_2 (which has the same symmetry as CO_2 and N_2O in its ground state) within the strong field approximation, namely $|F_{\|}(3,3,|1|,\Omega)| < |F_{\|}(1,1,|1|,\Omega)| < |F_{\|}(3,1,|1|,\Omega)|$ [23, 24]. The involvement of non-negligible electronic angular momenta (here *l* up to 3 with significant amplitude) in the continuum electronic dynamics is the reason why fractional revivals such as

1/12 and 1/6 for CO_2, and 1/3 and 1/6 for N_2O, are conspicuous in the HHG signals. These are associated with higher order rotational moments (such as $\left\langle \cos^4\theta \sin^2\theta \right\rangle$ in the present example), which allow for high order rotational coherences and hence high order fractional rotational revivals.

To physically interpret our results, each electronic dipole matrix element $F_{\parallel(\perp)}(l,l',k_l,\Omega)$ can be translated into an underlying dynamical event. For molecules such as N_2, the bound σ_g state can be written as a superposition of electronic angular momentum states *l=0*, *l=2*, *l=4*, where the *l=0* state strongly dominates and the *l=4* contribution is very small. This bound state undergoes ionization primarily to the *l=1* continuum state. Even if the free electron gains angular momentum in the strong field, dipole selection arguments in the recombination step strongly favor processes where the *l=1* continuum electron recombines to the *l=0* electronic angular momentum state (i.e. angular momentum conserving trajectories). In molecules such as O_2, N_2O and CO_2, the bound (π_g) state can be written as a superposition of electronic angular momentum states *l=2*, *l=4*, and the *l=2* state strongly dominates. This state ionizes to make predominantly the *l=1* continuum state (with smaller contributions from *l=3* and *5*). While travelling in the continuum, the electron can gain angular momentum from the photon field. In this case, because the *l=0* state is not occupied, recombination must occur predominantly into *l=2*, from either the *l=1* or *l=3* states (i.e. angular momentum conserving and non-conserving trajectories). The dominating *F(l'=1, l=3)* dipole therefore includes the interference of two quantum pathways. Thus, in the case of O_2, N_2O and CO_2, the dipole recombination selection rules do not conceal the continuum electron dynamics, allowing us to see that what the electron really wants to do is to gain angular momentum from the photon field (shown schematically in Figure 3(c)).

The picture that emerges thus associates with the high order rotational expectation values an interesting interplay between strong field electron dynamics and angular momentum propensities. In particular, the high order rotational expectation values are enabled by transitions from higher angular momentum states of the continuum states to the ground state of the molecule. Each of these high order moments, in turn, can be linked to a given high order fractional revival in the HHG spectrum. In this way the electronic dynamics expresses itself in the experimental observable. Thus, the rotational revival structure contains rich information not

only about the rotational coherences but also about the attosecond electronic motions, which can be extracted from a fit of an exact theory to high quality experimental data.

Our results suggest a range of new and fascinating opportunities that can be explored. For example, more information about electronic dynamics could be gained from the phases of the electronic matrix elements. Our theory can readily extract these phases from data, but this requires measurements not only of the harmonic intensities but also of their phases at the high order fractional revivals, which are challenging. Moreover, an interesting controversy in HHG from aligned molecules is the role played by multiple orbitals. For CO_2, the conclusions of Ref. [29] are in striking contradiction with those of Refs. [30, 31]. Our approach could be readily extended to explore the role of multiple orbitals .

The authors gratefully acknowledge the help of Dr. Maxim Artamonov. They thank the DOE Office of Basic Energy Sciences (grants numbers DE-FG02-99ER14982 and DE-FG02-04ER15612) and the AFOSR (grant number P.O. 217178/01 // FA9550-11-1-0001) for support, and the NSF EUV ERC for use of facilities.

Figure captions

Fig. 1. Normalized experimental HHG intensity (solid black) and fits to the two-center interference model integrated with the alignment distribution (dashed red) along with fits to the exact theory of [23, 24] (dotted blue) for the 31st harmonic from CO_2 for (a) the full rotational period and (b) for the time period indicated by the dashed black box in (a).

Fig. 2. Normalized experimental HHG intensity (solid black) and fits to the two-center interference model integrated with the alignment distribution (dashed red) along with fits to the exact theory of [23, 24] (dotted blue) for the 25th harmonic from N_2O for (a) the full rotational period and (b) for the time period indicated by the dashed black box in (a).

Fig. 3 Fundamental electronic dipole elements versus the harmonic order for (a) CO_2 and (b) N_2O for $|F_{||}(1,1,k_l,\Omega)|$ (black squares), $|F_{||}(3,1,k_l,\Omega)|$ (red circles), and $|F_{||}(3,3,k_l,\Omega)|$ (green triangles). $F_{||}(l,l',k_l,\Omega)$ signifies ionization parallel to the molecular axis into a continuum state with angular momentum l', propagation in the field, followed by recombination into the ground state from a continuum state of angular momentum l. (c) Schematic illustrating an electron trajectory in the continuum where an electron undergoes tunnel ionization from the $l=2$ electronic state of the molecule, emerges in the continuum in an $l=1$ state where it gains angular momentum, and then finally recombines from an $l=3$ state back into the ground electronic state of the molecule.

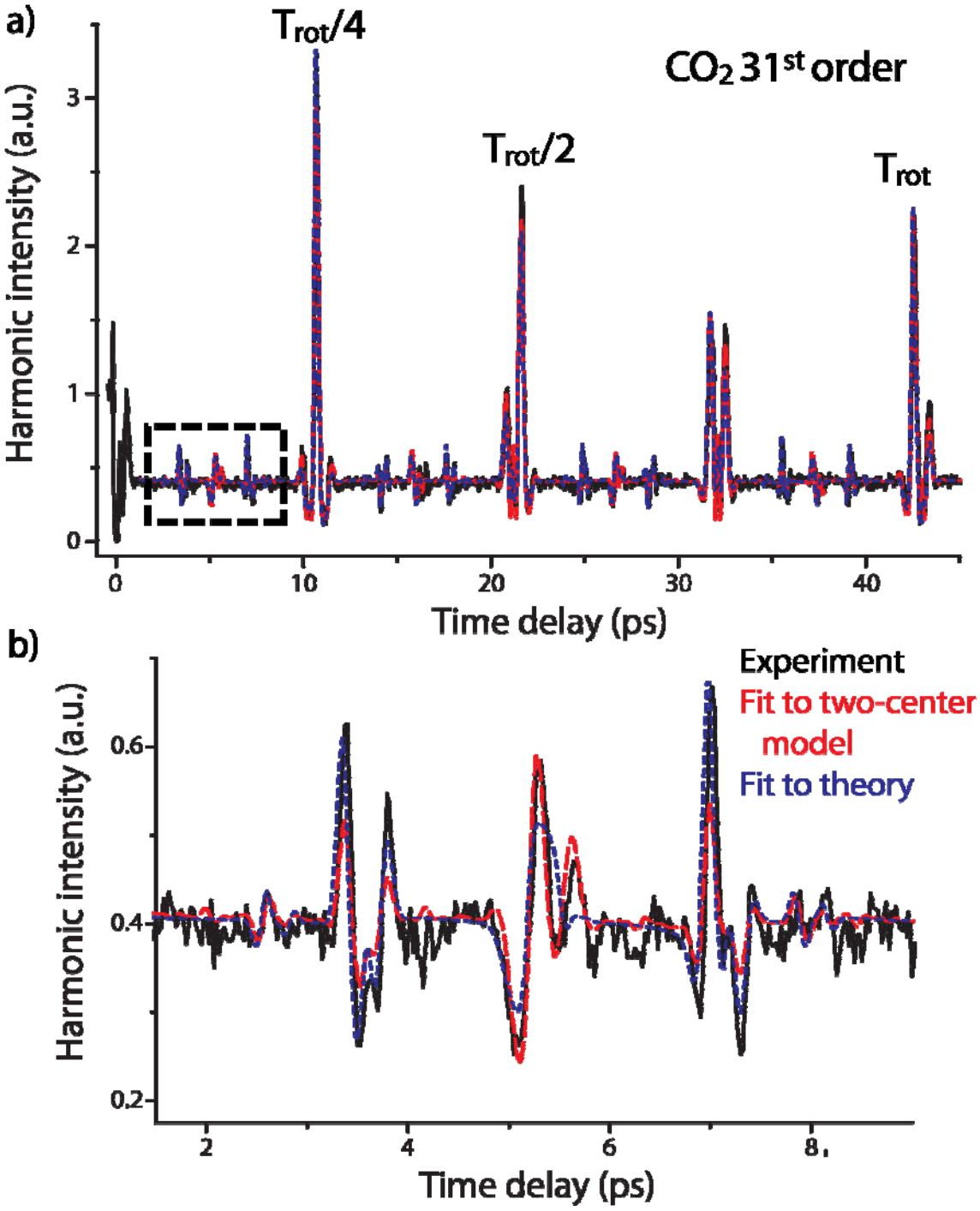
a)
$T_{rot}/4$
CO_2 31st order
$T_{rot}/2$
T_{rot}
Harmonic intensity (a.u.)
Time delay (ps)
b)
Experiment
Fit to two-center model
Fit to theory
Harmonic intensity (a.u.)
Time delay (ps)

Figure 1

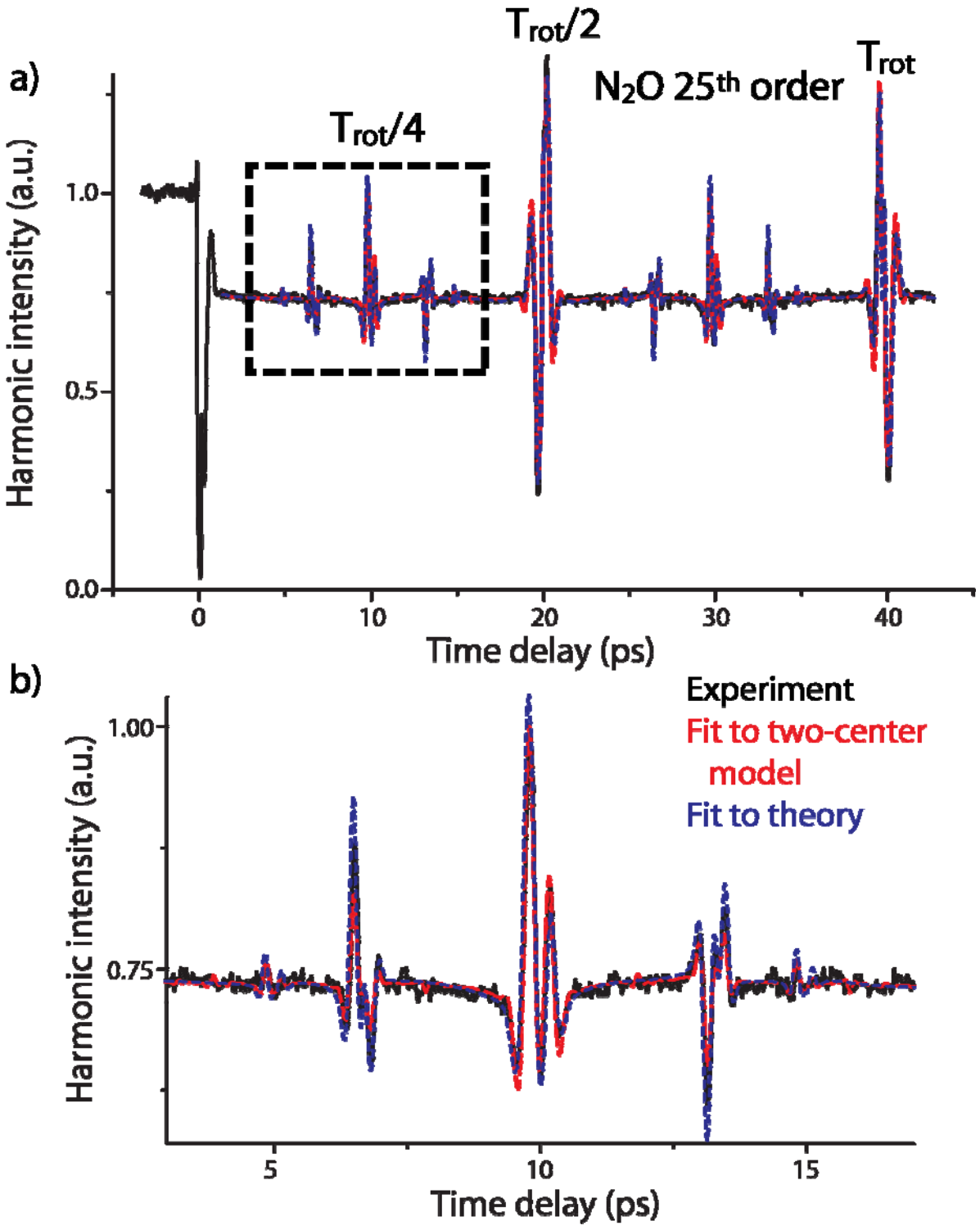
a)
Harmonic intensity (a.u.)
1.0
0.5
0.0
0
10
20
30
40
Time delay (ps)
$T_{rot}/2$
$T_{rot}/4$
T_{rot}
N_2O 25th order
b)
Harmonic intensity (a.u.)
1.00
0.75
5
10
15
Time delay (ps)
Experiment
Fit to two-center model
Fit to theory

Figure 2

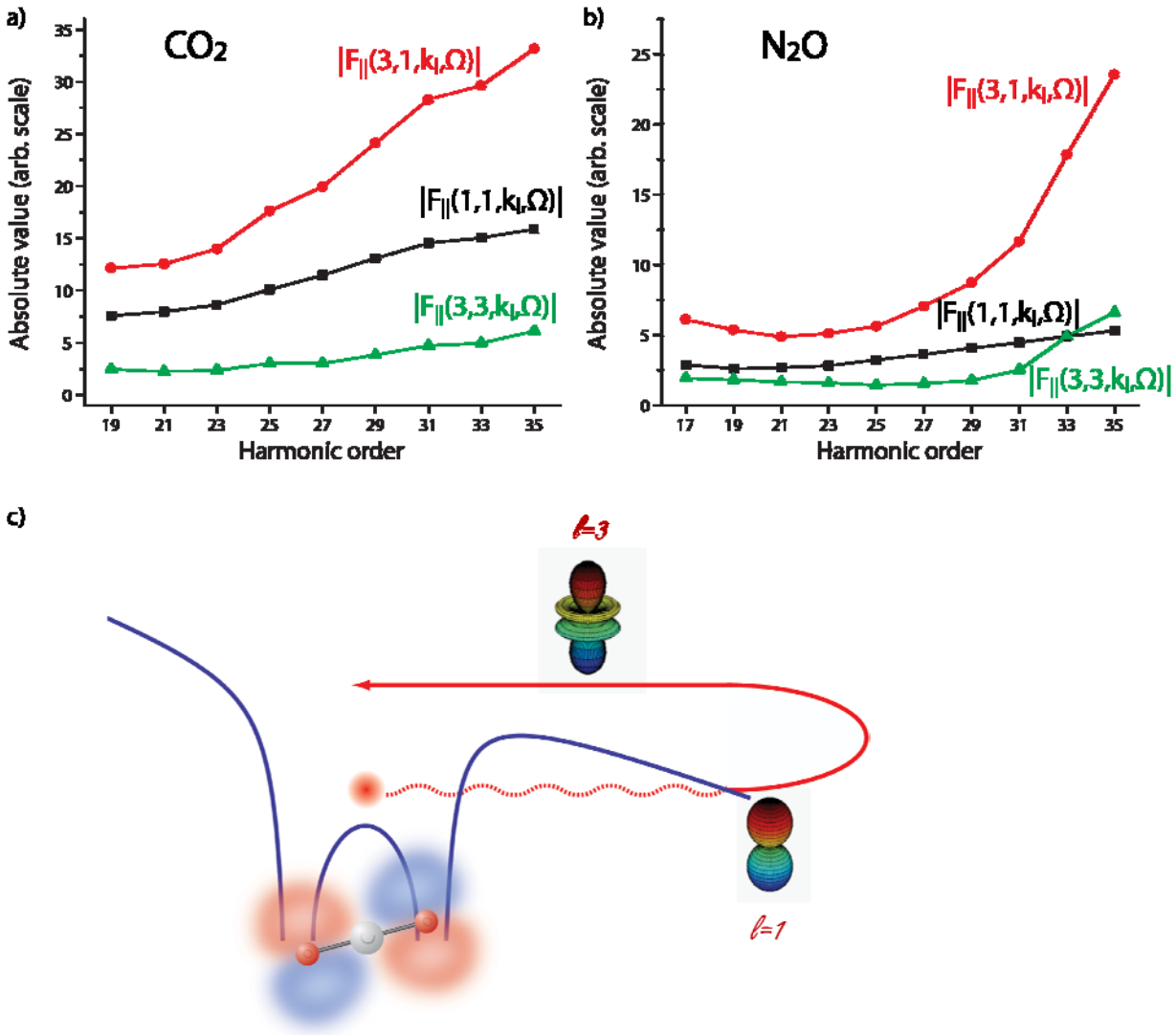
a)
CO2
F		(3,1,kl,Ω)
F		(1,1,kl,Ω)
F		(3,3,kl,Ω)
Absolute value (arb. scale)
Harmonic order
b)
N2O
F		(3,1,kl,Ω)
F		(1,1,kl,Ω)
F		(3,3,kl,Ω)
Absolute value (arb. scale)
Harmonic order
c)
ℓ=3
ℓ=1

Figure 3

References

[1] J. Itatani *et al.*, Nature (London) **432**, 867 (2004).
[2] J. Itatani *et al.*, Phys. Rev. Lett. **94**, 123902 (2005).
[3] C. Vozzi *et al.*, Phys. Rev. Lett. **95**, 153902 (2005).
[4] T. Kanai *et al*., Nature (London) **435**, 470 (2005).
[5] N. L. Wagner *et al.*, Proc. Natl. Acad. Sci. USA **103**, 13279 (2006).
[6] S. Baker *et al.*, Science **312**, 424 (2006).
[7] N. Wagner *et al.*, Phys. Rev. A **76**, 061403 (2007).
[8] R. Torres *et al.*, Phys. Rev. Lett. **98**, 203007 (2007).
[9] X. B. Zhou *et al.*, Phys. Rev. Lett. **100**, 073902 (2008).
[10] W. Li *et al.*, Science **322**, 1207 (2008).
[11] N. Kajumba *et al.*, New J. Phys. **10**, 025008 (2008).
[12] W. Boutu *et al.*, Nature Phys. **4**, 545 (2008).
[13] B. K. McFarland *et al.*, Science **322**, 1232 (2008).
[14] X. B. Zhou *et al.*, Phys. Rev. Lett. **102**, 073902 (2009).
[15] R. M. Lock *et al.*, Chem. Phys. **366**, 22 (2009).
[16] R. Torres *et al.*, Phys. Rev. A **81**, 051802(R) (2010).
[17] R. Torres *et al.*, Opt. Exp. **18**, 3174 (2010).
[18] H. J. Worner *et al.*, Nature (London) **466**, 604 (2010).
[19] T. Seideman, and E. Hamilton, Adv. At. Mol. Opt. Phys. **52**, 289 (2006).
[20] H. Stapelfeldt, and T. Seideman, Rev. Mod. Phys. **75**, 543 (2003).
[21] T. Seideman, Phys. Rev. Lett. **83**, 4971 (1999).
[22] M. Lewenstein *et al.*, Phys. Rev. A **49**, 2117 (1994).
[23] S. Ramakrishna, and T. Seideman, Phys. Rev. Lett. **99**, 113901 (2007).
[24] S. Ramakrishna, and T. Seideman, Phys. Rev. A **77**, 053411 (2008).
[25] P. Balcou *et al.*, Phys. Rev. A **55**, 3204 (1997).
[26] M. Lein *et al.*, Phys. Rev. Lett. **88**, 183903 (2002).
[27] M. Lein *et al.*, Phys. Rev. A **66**, 023805 (2002).
[28] A. Abdurrouf, and F. H. M. Faisal, Phys. Rev. A **79**, 023405 (2009).
[29] O. Smirnova *et al.*, Nature (London) **460**, 972 (2009).
[30] C. Vozzi *et al.*, Nature Phys. **7**, 822 (2011).
[31] K. Kato *et al*., Phys. Rev. A **84**, 021403(R) (2011).